Research Article

Long Chen*, Qingbao Yang, Xue Yang, Zhanqiang Liu, and Qinghua Song

An investigation on thermo-mechanical performance of graphene-oxide-reinforced shape memory polymer

https://doi.org/10.1515/ntrev-2022-0133
received March 14, 2022; accepted May 15, 2022

Abstract: Based on micro morphology, a thermo-mechanical coupling model of shape memory graphene oxide/epoxy resin (SMGO/EP) was proposed. The heat transfer capability, mechanical property and shape memory ability of shape memory polymer (SMP) were further investigated. The reliability of the modeling was verified by comparing the heat transfer and shape fixation rate of the experimental and simulation data. The results showed that the maximum error of heat transfer was 6.04%, and shape fixing rate error was 2.33%. When the volume fraction of GO was 1.50 vol%, the maximum stress can reach 158.39 MPa, 46.52% higher than that of pure shape memory EP. With the increase in the volume fraction of GO in the SMGO/EP composites, the heat transfer enhancement and recovery rate of SMGO/EP were directly affected by the doping content of GO. The surface temperature of the composites with GO doping content of 1.50 vol% was 20.26°C higher than that of pure SMEP after heating for 300 s. Under the coupling effect of heat transfer and stress characteristics, the mechanism of shape memory effect of SMGO/EP composites was revealed. The thermo-mechanical coupling modeling of SMGO/EP can effectively predict the shape memory characteristics of the SMGO/EP composites.

*** Corresponding author: Long Chen,** School of Mechanical Engineering, Key Laboratory of High Efficiency and Clean Mechanical Manufacture of MOE, Shandong University, Jinan, China; School of Mechanical Engineering, Shandong University, Jinan, China; School of Mechanical Engineering, Key Laboratory of Icing and Anti/De-icing, China Aerodynamics Research and Development Center, Mianyang, China, e-mail: 812612937@qq.com
Qingbao Yang, Zhanqiang Liu, Qinghua Song: School of Mechanical Engineering, Key Laboratory of High Efficiency and Clean Mechanical Manufacture of MOE, Shandong University, Jinan, China; School of Mechanical Engineering, Shandong University, Jinan, China
Xue Yang: School of Mechanical Engineering, Jilin Province Electric Power Research Institute Co., Ltd, Changchun, China

Keywords: graphene oxide, thermo-mechanical, heat conduction, microstructures, shape memory

1 Introduction

Shape memory material (SMM) plays an important role in the field of intelligent materials. Its characteristic is that it has a certain initial shape, after deformation and fixed into another shape, it can sense the changes in specific external conditions (such as temperature, chemical, mechanical, optical, magnetic or electrical, and other external stimuli), so as to return to the initial state [1–4]. SMMs can be divided into shape memory alloy (SMA) [5–9], shape memory ceramic (SMC) [10–13], and shape memory polymer (SMP) [14–20]. Compared with SMA and SMC, SMP has the advantages of high shape recoverability (~100%), stable shape fixity (more than 85%) and light weight (no more than 5 g/cm^3) [21,22], so they become the main research direction of shape memory material in the future.

Many scholars have investigated the shape memory properties of shape memory epoxy resin (SMEP) [23–25]. Liu *et al.* [26] prepared the SMEP samples, and the results showed that the SMEP had high shape fixation rate (99.50%) and shape recovery rate (~100%), and the glass transition temperature measured by differential scanning calorimetry was between 44.70 and 145.30°C. Wu *et al.* [27] successfully synthesized a new type of SMEP whose storage modulus ratio of the glassy state to the rubberized state was up to 400. After 6 test cycles, the shape fixity rate and shape recovery rate were maintained at about 99%. Sun *et al.* [28] prepared SMEP by two-stage curing method, and found that the exceptional shape memory properties of EP system can be maintained after the first stage curing. The tensile strength of the material can be effectively strengthened after the second stage curing.

However, the thermal stability, strength, and stiffness of pure shape memory polymer materials are relatively low, which greatly reduces the scope of its

application [29–33]. For the sake of the better thermal and mechanical properties, relevant scholars try to enhance the mechanical strength and thermal stability of raw materials by adding some reinforced fillers, such as SiC [34], Fe_3O_4 [35], glass fiber [36,37], carbon fiber [38], carbon nanotubes (CNTs) [39,40], and graphene [41,42]. Compared with pure SMEP, the strength and Young's modulus of CNTs/EP composite films prepared by Liu *et al.* were significantly improved [43]. Datta *et al.* [44] incorporated CNT film into SMEP to enhance shape memory CNT/SMEP composites. Compared with SMEP, the Young's modulus of the shape memory CNT/SMEP composites increased by 52 and 514% at 25 and 50°C, respectively. The storage modulus also improved significantly and the increase range was between 60 and 82% in the range of 30–90°C. Wang *et al.* [45] prepared a novel ternary hybrid polymer shape memory composites composed of GO, CNTs, and waterborne epoxy resin (WEP). The data results indicated that GO and CNTs had synergistic effect on improving the thermal response speed, tensile strength, and thermal conductivity of the composites. It was the uniform dispersion of CNTs and the strengthening effect of GO that created the synergistic effect. Liu *et al.* [46] obtained SMEP composites (SMEPC) with excellent mechanical properties by introducing carbon fibers into pure SMEPC. The storage modulus of SMEPC is as high as 37 GPa at ambient temperature, and the maximum resilience is more than 4.40 GPa. Lu *et al.* studied the synergistic effect of self-assembled carboxylic acid-functionalized carbon nanotube (CNT) and carbon fiber [47], self-assembly multi-walled carbon nanotube (MWCNT) nanopaper and sub-micro nickle nanostrand [48] on the electrical properties and electro-active recovery behavior respectively. The vertically aligned nickel nanostrands will facilitate the heat transfer from the nanopaper to the underlying SMP composite to accelerate the electrical actuation. While the self-assembled carboxylic acid-functionalized CNTs and carbon fibers enable the SMP nanocomposites for Joule heating triggered shape recovery.

Graphene has exceptional properties in optics, electricity, and mechanics. It has important application prospects in materials science, micro-nano processing, and energy, because of which it is considered to be a revolutionary material in the future [49,50]. Yu *et al.* [51] studied the influence of GO content on epoxy polymer composites by doping different amounts of GO to SMEP. The results showed that when the mass fraction of GO was 0.80 wt%, the shape memory composites had extraordinary shape memory performance. Chen *et al.* [52] discussed the effect of thermally reduced graphite oxide (TrGO) content on the mechanical and thermal properties and shape memory behavior of TrGO/EP. The static mechanical tests showed that the addition of TrGO can significantly improve the Young's modulus, tensile strength, flexural modulus, and flexural strength of EP. Comprehensively considering the mechanical properties and shape memory effect of TrGO/ESMP composite, the optimum TrGO content was 2 wt%. Wang *et al.* [53] prepared a novel thermoelectric response shape memory graphene/WEP composite. With the raise in the graphene content and temperature, the thermal active shape memory effect became better. The shape recovery rate of the composites was still more than 95% and the number of fold-unfold cycles had a small effect on the shape memory properties. Wang *et al.* [54] prepared a new type of rGO/EP/rGO sandwich structure composite film. The thermal response shape recovery process of the sample can be completed in only 3 s in hot water at 80°C. The above results show that the addition of rGO can optimize the performance of SMEP.

Simulating the shape memory process of materials by numerical simulation software has significant advantages in the in-depth study of thermo-mechanical coupling mechanism. Liu *et al.* [55] introduced in detail the integral hinge manufactured from carbon-fiber-reinforced SMEP, and obtained the elastic modulus of SMPC varying with temperature through tensile test. The results showed that the hinge had satisfactory shape memory recovery performance, including a 100% shape recovery rate after 10 fold-unfold cycles, and a shape recovery time of about 60 s from 180° to 0°. Based on the Neo-Hookean constitutive equation considering the time-temperature effect, Fan *et al.* established the tensile stress and strain expressions of thermal shape memory process [56]. The shape memory experiment was constructed by employing SMEP to calibrate the viscoelastic parameters, and the shape memory process under bending and torsion was successfully simulated to verify the reliability of the numerical method. Diani *et al.* [57] measured the viscoelastic behavior of SMEP and its correlation with time and temperature by dynamic mechanical analysis (DMA). The generalized Maxwell model was used to model the amorphous thermal solid under study. The viscoelastic behavior of the amorphous thermal solid was described by DMA experimental data and time-temperature superposition principle. The simulation results were in good accordance with the experimental data, which showed that the shape recovery time of amorphous polymer was related to temperature.

At present, most of the work only studied the shape memory properties of shape memory polymer composite, but the mechanism of the effect of GO doping on the thermal-mechanical coupling enhancement of SMEP has not been clarified. What's more, the influence of GO doping on SMGO/EP's heat transfer capability and mechanical

property was also rarely mentioned. Therefore, based on the micro morphology characterization, a thermal-mechanical coupling numerical simulation model of SMGO/EP composite was established. The influence of shape memory performance of SMGO/EP composite with different volume fractions of GO was analyzed by finite element method. The relationship between shape memory effect and thermal properties of SMGO/EP was studied. The reliability of numerical simulation data was verified by experiments. Through the simulation results, the promotion of GO doping on heat transfer, mechanical properties and shape memory properties was hope to see.

2 Experimental setup

In this section, the principle and method of SMGO/EP composite preparation were introduced, and the cross section of SMGO/EP composite was characterized by scanning electron microscope (SEM). In addition, the verification experiment platform was set.

2.1 Materials

The materials used in this experiment included epoxy resin (E-51), provided by Shanghai Autun Chemical Technology Co., Ltd. GO was provided by Tanfeng Tech. Inc., with a lamellar diameter of 0.20–10 μm, layer number of 1–20, and a purity of ~98%. The curing agent was employed as 4,4-Diaminodiphenylmethane ($C_{13}H_{14}N_2$), which was purchased from Shanghai Zhanyun Chemical Co., Ltd. The dispersant was ethanol absolute (C_2H_6O), which was purchased from Wuxi Zhanwang Chemical Co., Ltd.

2.2 Preparation of SMGO/EP composites

The SMGO/EP composite sample in the experiment was composed of EP and GO. A certain quality of GO was weighed and dispersed in ethanol absolute for 15 min. The GO was mixed with preheated EP and then the mixture was uniformly dispersed for 30 min to prevent GO from agglomerating. The well-mixed mixture was put into the blast drying box and vacuum oven for 2 h, respectively, to remove the bubbles in the mixture. In this period, the carboxyl group of GO made the epoxy group ring open. Finally, the curing agent was added to the mixed liquids and stirred for about 10 min, and the mixed liquids was poured into the mold with dimension of 90 mm × 20 mm × 3 mm. The curing process was performed in a vacuum oven for 2.50 h at 80°C and 2 h at 150°C. The whole reaction process was shown in Figure 1. Red, blue and white spheres represented shape memory EP, GO and curing agent respectively After GO was mixed with shape memory EP, the oxygen-containing functional groups on the surface of GO will react with the groups of shape memory EP to form ester groups. Then the curing agent made the EP group ring open.

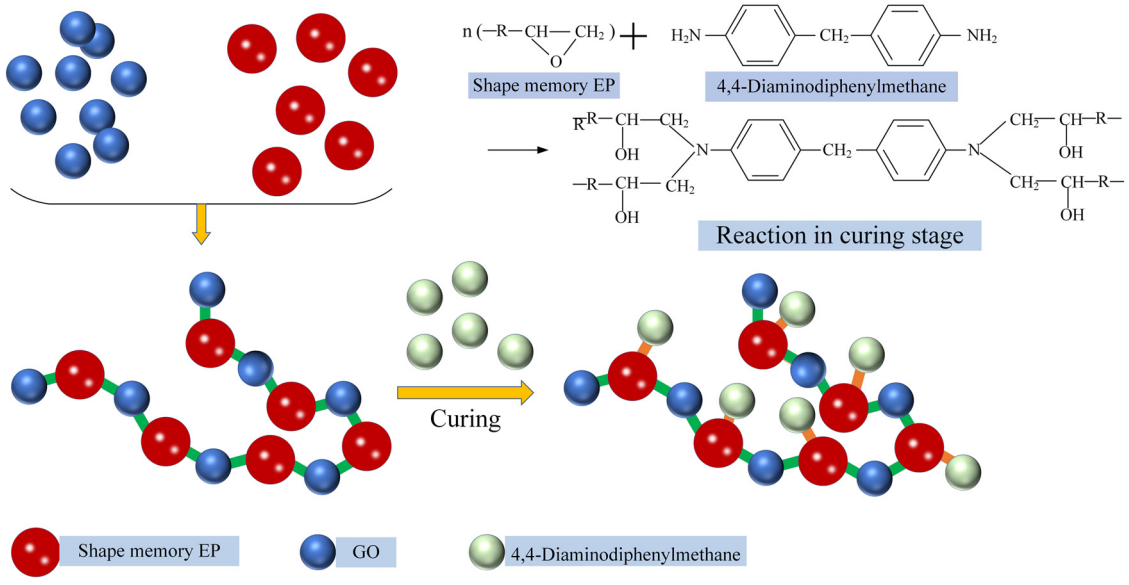

Figure 1: Schematic of reaction mechanism during preparation of SMGO/EP composites.

2.3 Characterization

In order to characterize the microstructures of SMGO/EP composites, SEM (Hitachi SU-8010) was adopted. As can be seen in Figure 2, with the raise in GO doping content, the fracture cross-section of SMGO/EP composites became coarser, and the cross-linking between GO and EP became more complex. The GO lamellae were evenly dispersed in the EP matrix, and there was no fold or separation in the contact between GO and EP, indicating that GO and EP had good interfacial compatibility.

2.4 Shape memory and heat transfer experiments

In order to verify the accuracy of the proposed simulation model, a SMGO/EP composite sample with volume fraction of 0.50 vol% of GO was prepared, and the experiment shown in Figure 3(a) was designed. During the deformation experiment, one end of the sample was horizontally fixed to the square table with a fixture, and the annular heating sleeve was fixed outside the sample to keep the sample temperature constant above the glass transition temperature (Figure 3[b]). The other end of the sample was slowly stretched at the speed of 0.50 mm/s through the electric push-pull meter to avoid breaking the sample due to large deformation. The maximum displacement of the push-pull meter was limited to 5 mm. After tensile deformation, the annular heating sleeve was removed to cool the sample to room temperature. The length of the sample was measured with a vernier caliper, and the shape fixation rate was calculated according to equation (10).

During the recovery process, the sample was heated above the glass transition temperature (T_g) to complete the thermal response shape memory recovery. The length of the sample was measured with a vernier caliper, whose accuracy was ±0.02 mm. During the measurement process, different positions of the sample were measured three times and the average value was taken to reduce the relative error of measurement. By comparing the experimental data with the simulation data, the error of the two groups of data was calculated to prove the reliability of the proposed modeling.

As shown in Figure 3(c), the prepared SMGO/EP composite sample was pasted on the heating pad with thermal

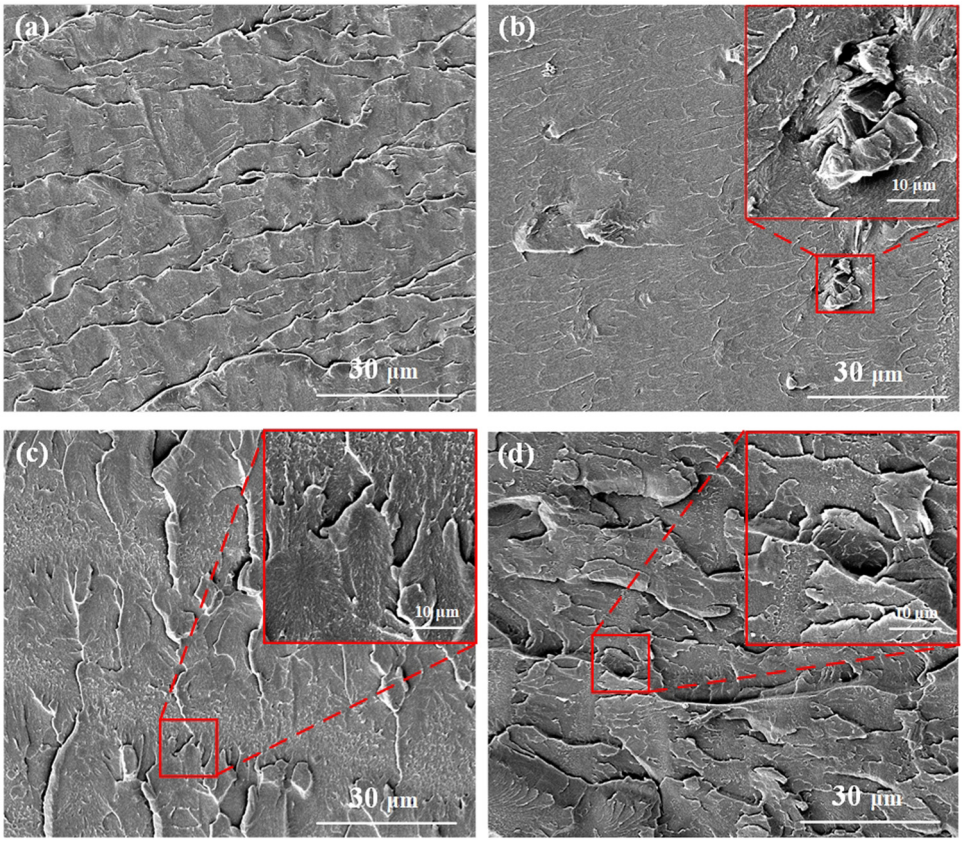

Figure 2: SEM images of SMGO/EP composites with the GO content of (a) 0 vol%, (b) 0.5 vol%, (c) 1.0 vol%, and (d) 1.5 vol%.

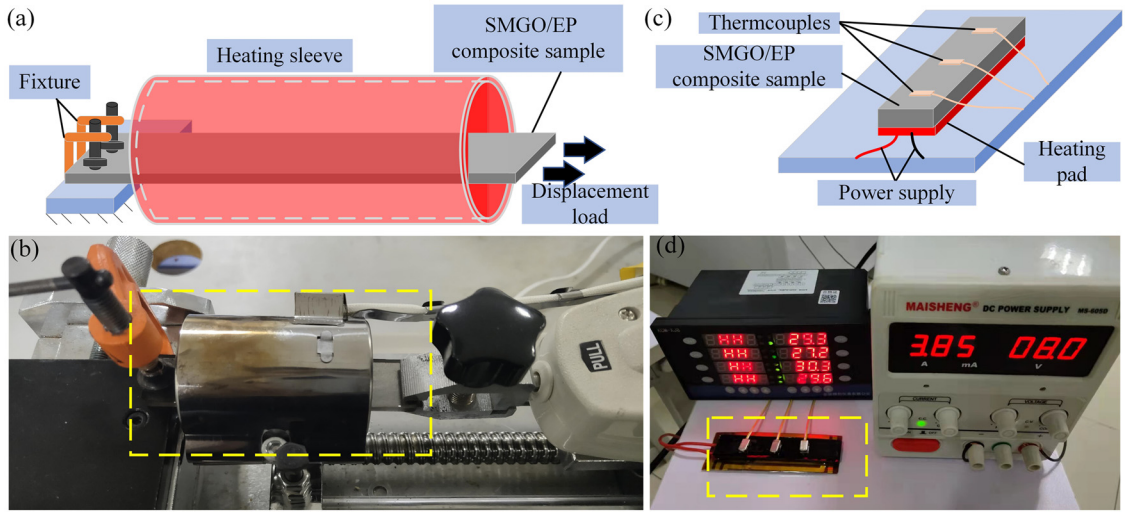

Figure 3: Schematics of (a) shape memory process, (b) heat transfer experimental devices of shape memory process, (c) and (d) heat sensor arrangement.

conductive adhesive without gap between them. The heat flux of the heating pad was adjusted through the external power supply, and the upper surface of the sample exchanged heat with the air naturally. Three K-type thermocouples were employed to measure the temperature data of fixed points on the surface of the sample (Figure 3(d)). The average values were compared with the numerical simulation data. The thermocouple sensor had a temperature range of 200–400 K and accuracy of ±0.50 K, including uncertainty caused by data acquisition software. The thermocouple was pasted on the outer surface of the experimental sample with a thermal conductivity of 3.60 W/(m K) and a thickness of 0.15 mm. The heating pad was externally connected with DC power supply (MS605dD) with rated voltage of 60 V to provide the heating conditions required for the experiment. The maximum error between the experimental temperature data and the simulation data was calculated.

3 Micro finite element simulation

The calculation principle of finite element simulation process was proposed. The three-dimensional model was established according to the SEM characteristics. The parameter selection and boundary condition setting during modeling process were performed.

3.1 Modeling

The shape memory process of SMGO/EP composites is closely related to the constitutive model. Viscoelasticity is the model form of shape recovery characteristics of polymer materials. The shape memory behavior of shape memory polymer materials is essentially the viscoelastic behavior of polymers. It is assumed that GO is uniformly distributed in SMEP, and SMGO/EP composite is regarded as a kind of isotropic material.

The deformation behavior of SMEP was simulated by employing the generalized Maxwell constitutive mode. Considering the thermal expansion effect of the material, the linear viscoelastic constitutive model and the time temperature equivalent principle were used to calculate the deformation behavior of SMEP. The stress response of polymer viscoelasticity included viscosity and elasticity. The elastic part responded immediately under the action of force, while the viscous part appears slowly after relaxation time. For linear isotropic viscoelastic mechanics, the constitutive relation formula equation (1) and the stress function integral formula equation (2) of the foundation are as follows [58,59]:

$$\dot{\varepsilon} = \frac{1}{E} \cdot \dot{\sigma} + \frac{1}{\eta} \cdot \sigma, \tag{1}$$

$$\sigma(t) = \int_0^t 2G(\tau - t')\dot{e}\mathrm{d}t' + I\int_0^t K(\tau - t')\dot{\phi}\mathrm{d}t', \tag{2}$$

where E and η represent the elastic modulus and viscosity of the material, respectively; $\dot{e}$ is the strain rate deviation of shear deformation; $\dot{\varphi}$ denotes the volume strain rate of volume deformation; $K(t)$ is the bulk modulus relaxation function, and $G(t)$ is the shear modulus relaxation function. $K(t)$ and $G(t)$ are functions of relaxation time τ. The relaxation time τ establishes the relationship with

the actual time t by the following integral equation (3) and differential equation (4):

$$\tau = \int_0^t \frac{\mathrm{d}t'}{A_T(T(t))}, \tag{3}$$

$$\frac{\mathrm{d}\tau}{\mathrm{d}t} = \frac{1}{A_T(T(t))}, \tag{4}$$

where T is the temperature and A_T is the transfer function. The Williams–Landel–Ferry (WLF) equation is a commonly used form of transfer function, which is the instantaneous temperature equivalent equation. When applied to polymers, the glass transition temperature T_g is usually used as the reference temperature. The specific form of WLF equation is shown as equation (5)[60], and the fitting results of relevant parameters in WLF equation are shown in Table 1.

$$\log A_T = -\frac{C_1^g(T - T_g)}{C_2^g + T - T_g}, \tag{5}$$

where C_1^g and C_2^g are constants of WLF equation, which is related to material. In the numerical simulation, the material has elastic deformation under the condition of $T \le T_g - C_2^g$.

In the numerical simulation, the $K(t)$ and $G(t)$ parameters describing the viscoelastic integral function are expressed in the form of Prony series. The values in Prony series are fitted by relaxation experiment, and the viscoelastic parameters are calculated by equations (6)–(9), as shown in Table 2.

$$G(t) = G_\infty + \sum_{i=1}^{n_G} G_i \mathrm{e}^{-t/\tau_i^G}, \tag{6}$$

$$K(t) = K_\infty + \sum_{i=1}^{n_K} K_i \mathrm{e}^{-t/\tau_i^K}, \tag{7}$$

Table 1: Fitting results of WLF parameters

Parameters	T_g	C_1^g	C_2^g
SMEP	100.00	17.44	51.60

Table 2: Fitting results of viscoelastic model parameters

SMEP	*g_i* Prony	*tau_i* Prony
1	0.86	0.1
2	0.07	1
3	0.05	10
4	0.005	100
5	0.003	1,000

$$k\_i = \frac{K_i}{K_0}, \tag{8}$$

$$g\_i = \frac{G_i}{G_0}, \tag{9}$$

where K_∞ and G_∞ denote the long-term bulk modulus and long-term shear modulus, respectively; τ_i^K and τ_i^G are the relaxation time of each Prony series. Usually, τ_i^K and τ_i^G are not equal, but it is assumed that $\tau_i = \tau_i^K = \tau_i^G$ in the numerical simulation; *k_i* and *g_i* represent the relative bulk modulus and relative shear modulus, respectively. In Prony series, the order of bulk modulus n_K and shear modulus n_G may not be the same. In fact, it can be assumed that $n_K = 0$ in the simulation.

SMGO/EP composite is a two-phase material, in which one is the homogeneous medium and the other represents a finite number of reinforced fillers [61]. The governing equation for the heat transfer analysis of the composite can be expressed as follows:

$$(\rho_i c_i)\frac{\partial T_i}{\partial \tau} = \nabla(k_i \nabla T_i) \text{ in } \Omega_i \ (i = 1, 2), \tag{10}$$

where T_i represents the average temperature, ρ_i denotes the material density, c_i represents the specific-heat, τ is the heat transfer time, k_i is the coefficient of heat transfer, $i = 1$ refers to the GO, and $i = 2$ refers to the SMEP. For the SMGO/EP composite, additional equation is needed to define the temperature and heat flux at the interfaces between GO and SMEP, which can be expressed as follows:

$$k_i \nabla T_i = h(T_2 - T_1) \text{ on } \Gamma_{12} \ (i = 1, 2), \tag{11}$$

$$k_i \nabla T_i = h(T_2 - T_1) \ (i = 1, 2). \tag{12}$$

where h denotes heat transfer coefficient indicating the interface thermal resistance when the heat is transferred from SMEP to GO.

The unit body taken from the SMGO/EP model can be considered as a thermodynamic system $\mathrm{d}V$, as can be seen in Figure 4. The heat flow is transferred from bottom to top along the z direction. The heat retained in the system per unit time along the z direction is as follows [62]:

$$Q_z = (q_z - q_{z+\mathrm{d}z})\mathrm{d}x\mathrm{d}y, \tag{13}$$

where q_z represents the input heat flux, $q_{z+\mathrm{d}z}$ represents the output heat flux.

The temperature field and heat flux are continuous in the SMGO/EP composite, and the equation can be written in the form of an expanded Taylor series at z, when the system $\mathrm{d}V$ tends to zero:

$$q_{z+\mathrm{d}z} = q_z + \frac{\partial q_z}{\partial z}\mathrm{d}z. \tag{14}$$

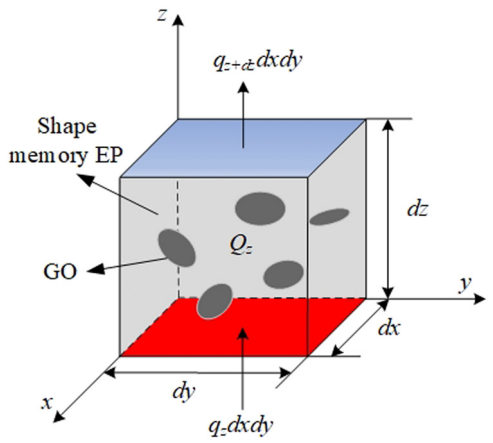

Figure 4: Energy conservation of a unit.

The Fourier's law is shown in equation (15). According to the equations (12)–(14), the energy generated inside the composite can be expressed as equation (16).

$$q_z = -\lambda \frac{\partial T}{\partial z}, \tag{15}$$

$$Q_z = \lambda \frac{\partial^2 T}{\partial z^2} \mathrm{d}z\mathrm{d}x\mathrm{d}y. \tag{16}$$

In the dV system, the increase in thermal energy per unit element is expressed as Q_1 and it can be calculated by equation (17). The heat transfers along the x, y direction are ignored, thus the heat transfer process can be approximated as one-dimensional heat conduction along z direction. There is no internal heat source inside the composite. Therefore, the heat conduction equation can be simplified as equation (18).

$$Q_1 = \rho c \frac{\partial T}{\partial \tau} \mathrm{d}x\mathrm{d}y\mathrm{d}z, \tag{17}$$

$$\lambda \frac{\partial^2 T}{\partial z^2} = \rho c \frac{\partial T}{\partial \tau}. \tag{18}$$

where λ is the thermal conductivity, ρ denotes the density, c represents the specific heat, t is the temperature, and τ is time.

For the natural convection heat transfer between the surface of SMGO/EP composite and the air, it follows Newton's cooling formula, as can be seen in equation (19). The surface heat transfer coefficient is affected by many factors. In this example, the average surface heat transfer coefficient is set as 20 W/(m^2 K) during the calculation.

$$q = h(t_w - t_f). \tag{19}$$

where t_w denotes the surface temperature, and t_f represents the air temperature.

3.2 Simulation process

The prepared samples of SMGO/EP composites were characterized by micro electron microscope. According to the characterization results, the three-dimensional geometric model of EP matrix and randomly distributed GO were generated by Python script file, as shown in Figure 5. The length, width, and height of SMGO/EP composites are 90 × 20 × 3 μm^3, respectively, and GO sheet with a diameter of ~1 μm. Then the size of the model is enlarged by 1000 times to compare with the experiment of the

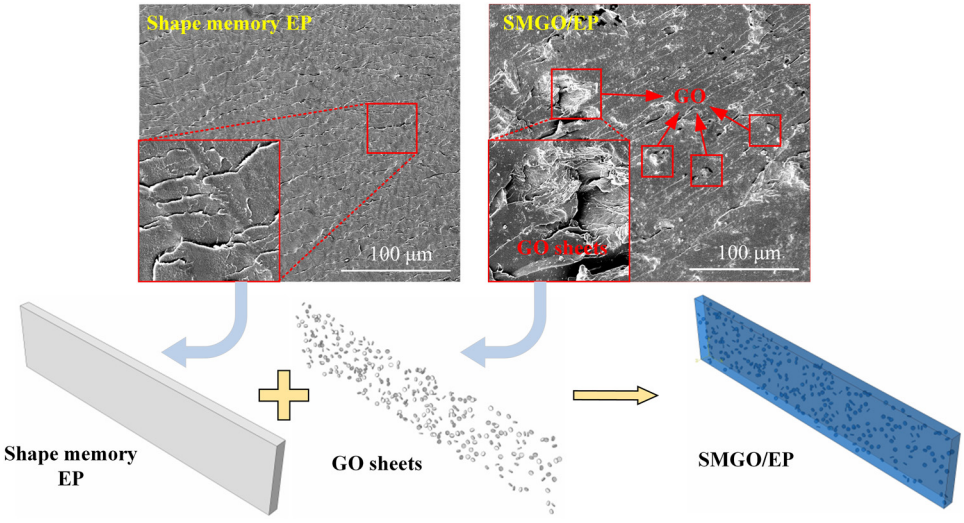

Figure 5: Micro modeling of SMGO/EP composites.

Table 3: Thermophysical parameters of SMEP

	Density (kg/m^3)	Specific heat (J/(kg K))	Conductivity (W/(m K))	Expansion coefficient (1/°C)
SMEP	1,500	530	0.363	6.470×10^{-5}

Table 4: Mechanical parameters of SMEP at different temperatures

Temperature (°C)	Young's modulus (MPa)	Poisson's ratio
40	1792.50	0.36
70	586.40	0.39
80	261.20	0.41
100	34.90	0.43

actual sample. According to the micromorphology relationship, the contact relationship between GO and EP was established. Tie contact mode was selected under the interaction module to transfer stress and heat through nodes. According to the experimental measurement and calculation, the material parameters of EP and GO were as shown in Tables 3 –5 [50] (Figure 6).

The overall shape memory process of the SMGO/EP composites was as shown in Figure 6. First, the sample was heated to above the glass transition temperature (set as 120°C) to make the composites in a high elastic state. The sample was fixed one end and the other end was stretched 5 mm with a speed of 0.05 mm/s. Then, cooled down to 30°C with a speed of 0.9°C/s and kept for a period of time to fix the shape of the SMGO/EP composites. After

Table 5: Thermophysical parameters of GO

	Young's modulus (GPa)	Poisson's ratio	Density (kg/m^3)	Specific heat (J/(kg K))	Conductivity (W/(m K))
GO	1,050	0.1866	1,500	700	4,840

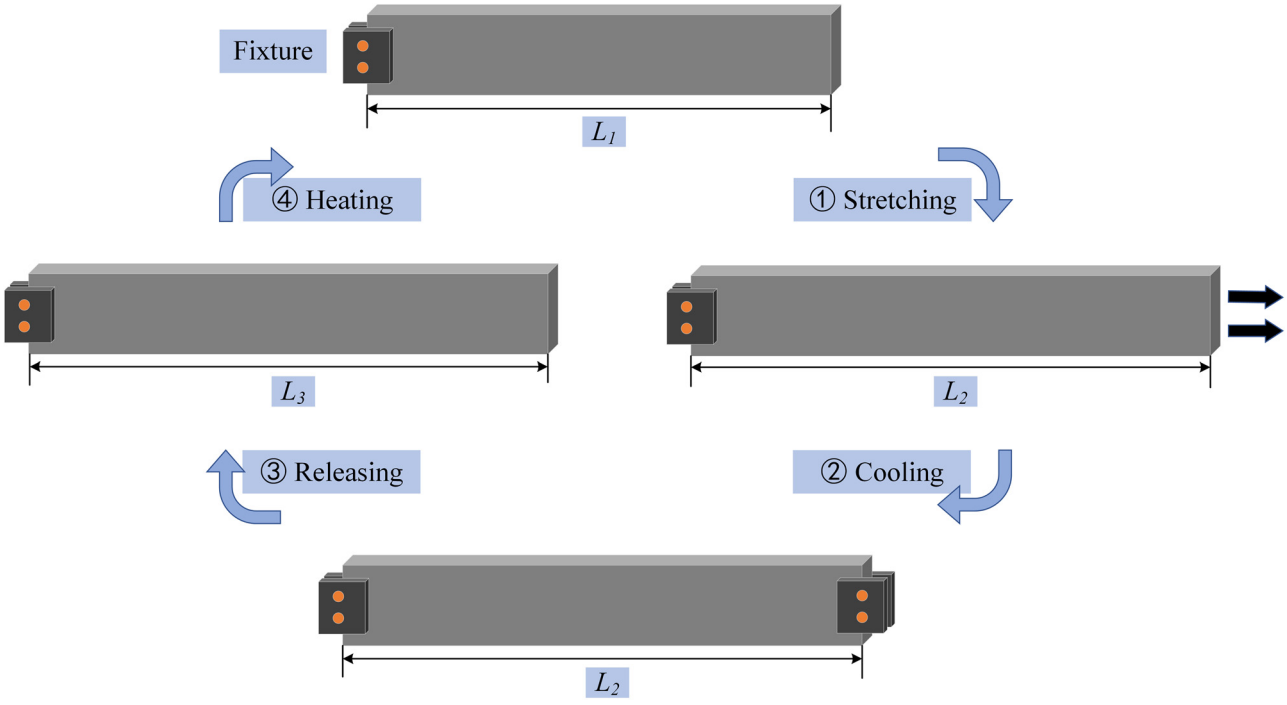

Figure 6: Schematic of shape memory process: (1) stretch 5 mm above the glass transition temperature with a speed of 0.5 mm/s; (2) cool down at a speed of 0.9°C/s and maintain a strain of 5 mm; (3) remove the displacement load; and (4) heat at a speed of 0.9°C/s.

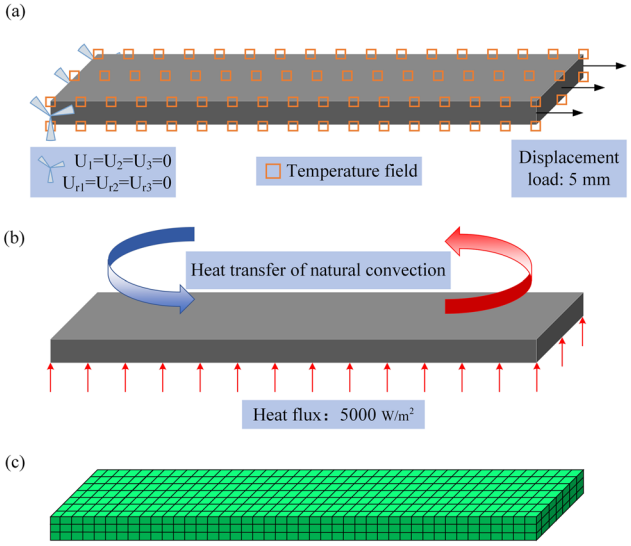

Figure 7: (a) Displacement boundary conditions and temperature field, (b) heat transfer boundary conditions, and (c) meshing of modeling.

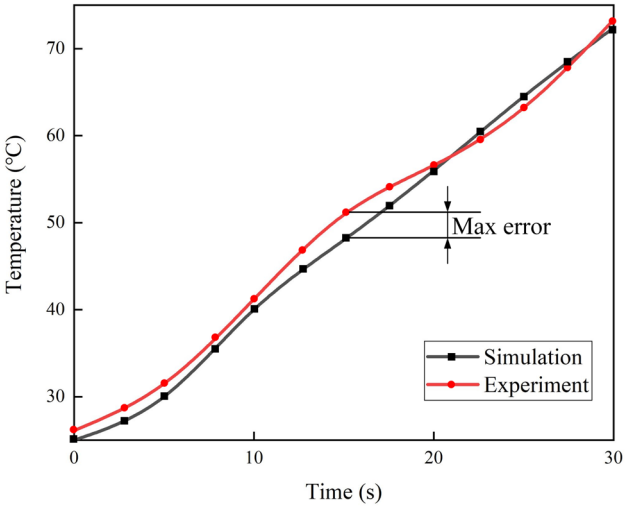

Figure 8: Comparison of experimental and simulation data.

the displacement load was removed, the sample was heated above the glass transition temperature with a speed of 0.9°C/s and returned to the initial state. The calculation formula equation (10) of the shape fixation rate R_f and shape recovery rate R_r are as follows, where L_1 denotes the initial length, L_2 represents the length after stretching, L_3 is the length after releasing, L_1' is the length of the SMGO/EP composites after shape recovery [63,64].

$$R_f = \frac{L_3 - L_1}{L_2 - L_1} R_r = \frac{L_2 - L_1'}{L_2 - L_1}. \quad (20)$$

3.3 Boundary condition and meshing

The stress–strain distribution of the shape memory process of the established model was calculated by visco analysis step. The setting of boundary conditions is shown in Figure 7(a). The grid element type of this process was eight node hexahedral linear reduction elements (C3D8R). The approximate global size was ~1 mm, and the number of grids was 5,400. The heat transfer analysis step was employed to calculate the heat transfer of the model. By applying an external heat source with the size of 5,000 W/m^2 on one side of the model, the boundary condition of the other side was heat transfer of natural convection. The boundary conditions were set as shown in Figure 7(b). The heat transfer analysis step was used to calculate the temperature field and heat flux distribution of the composite shape memory process. The grid element type adopted eight node heat transfer solid elements (DC3D8), the approximate global size was ~1 mm, and the number of grids is 5,400. The schematic of mesh dividing is shown in Figure 7(c).

4 Results and discussion

In this article, the correctness of the simulation results was verified by the experimental results. The shape memory performances, and thermal and mechanical properties of the SMGO/EP composites were studied by extracting the simulation data results.

4.1 Experimental validation

To verify the correctness of the simulation results, the SMGO/EP composite sample with a volume fraction of 0.50 vol% GO was prepared. The experiments shown in

Table 6: Simulation and experimental comparison of shape memory characteristics

	Retraction distance (mm)	Shape fixation rate (%)	Shape recovery rate (%)
Experimental	0.71	86.00	100
Simulation	0.61	87.80	99.99

Figure 3 were performed, and the results were measured and shown in Table 6. After the displacement load was removed, the sample retracted 0.71 mm, the shape fixation rate of the composite was 85.80%, which was close to the shape fixation rate obtained by simulation (87.80%), and the relative error was only 2.33%. It was considered that the experimental results were reliable within the allowable error range. After reheating, it was observed and measured that the SMGO/EP composites basically returned to the initial state, and the shape recovery rate was 100%.

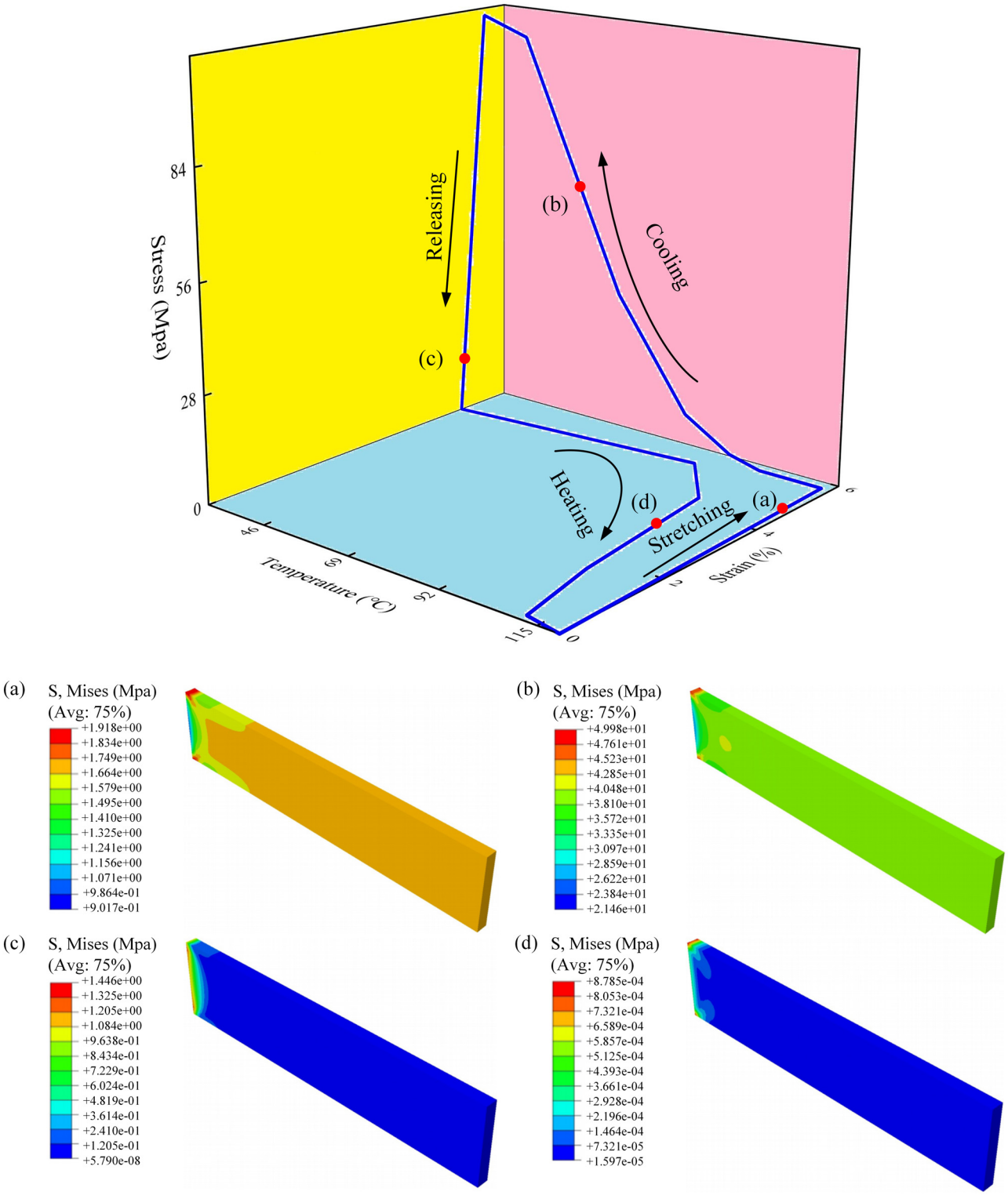

Figure 9: Three-dimensional curve of stress-strain-temperature and (a) to (d) stress distribution at state (a) to (d) of stress-strain-temperature curve.

Similarly, the prepared SMGO/EP composite samples with 0.50 vol% GO doping were tested for heat transfer characteristics. The experimental results are shown in Figure 8. The heating trend was consistent. The max relative error between the experimental and simulation values was the largest when heated to 15 s, and the max error was only 6.04%. The comparative data showed that the simulation error was within the allowable range, so that the simulation result was considered to be reliable.

4.2 Shape memory performance

The mechanical properties of shape memory epoxy resin are closely related to temperature, thus the coupling relationship between stress, strain, and temperature must be considered in order to accurately and completely reflect the shape memory process of SMGO/EP composites.

As shown in Figure 9, the three-dimensional schematic diagram of the stress-strain-temperature relationship of shape memory epoxy resin was obtained through numerical simulation calculation. It can be seen that above the glass transition temperature (T_g), the SMGO/EP composites were in a high elastic state. At this time, the elastic modulus was small, and the stress and strain in the tensile process were directly proportional, but the changes were not obvious. In state (a), the maximum difference of Mises stress was 0.90 MPa and the average stress was 1.66 MPa regardless of the stress concentration, as shown in Figure 9(a).

As the temperature decreased below the glass transition temperature (T_g), the stress increased significantly due to the increase in elastic modulus. In state (b) of the cooling period, the maximum difference of Mises stress increased to 25.82 MPa and the average stress was 38.10 MPa regardless of the stress concentration, as shown in Figure 9(b). At the moment after the displacement load was removed, the

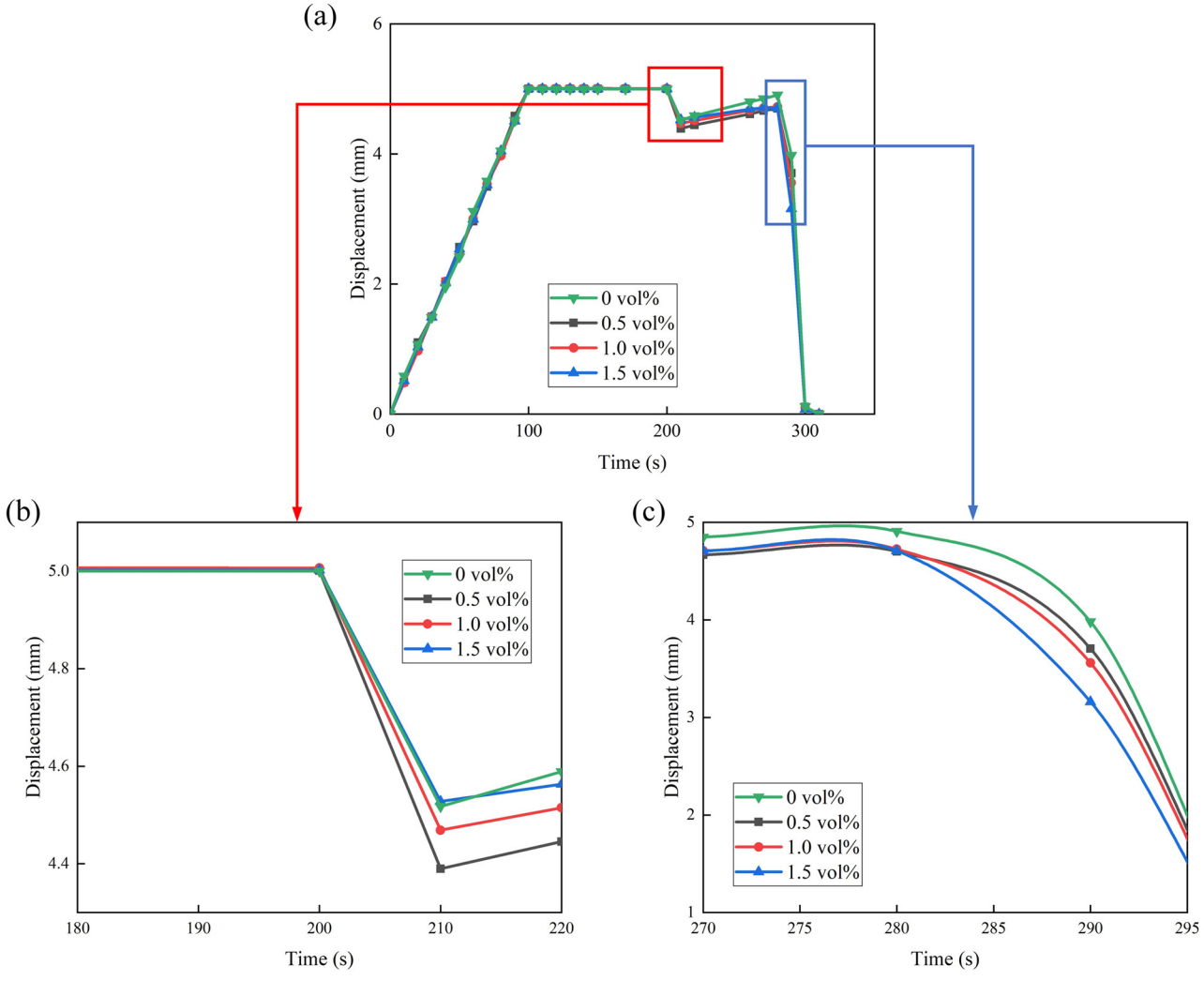

Figure 10: Displacement-time relationship: (a) 0–300 s, (b) 180–220 s, and (c) 270–295 s.

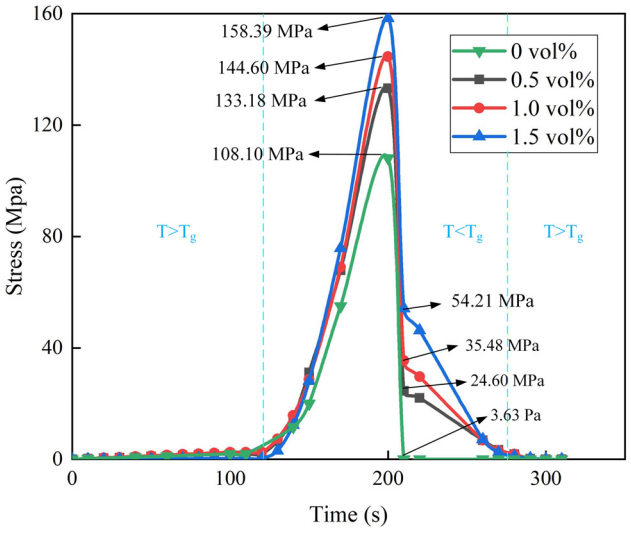

Figure 11: Stress distribution of SMGO/EP with different GO contents.

SMGO/EP composites rebounded and contracted with small displacement. During this period, the stress existed only where the stress was concentrated and the maximum Mises stress was only 1.45 MPa in state (c), as shown in Figure 9(c). In the subsequent heating process, the SMGO/EP composites were expanded by heating. When the sample was heated above the glass transition temperature, the composite quickly recovered its original shape. And the stress of the material was close to 0 in this period, as can be seen in Figure 9(d).

As can be seen from Figure 10(a), due to the same displacement load, the displacement changes in SMGO/EP composites with different graphene oxide contents were the same in the first 200 s. As can be seen from Figure 10(b), after 200 s, with the removal of displacement load, SMGO/EP composites with different GO contents had different degrees of displacement retraction (0.40–0.60 mm), and the size of retraction displacement determined the shape fixation rate of composites.

After calculation, with the increase in GO volume fraction, the shape fixation rate of SMGO/EP composites increased from 87.80 to 90.56%. Only when the volume fraction of GO exceeded 1.50 vol%, the shape fixation rate of SMGO/EP composites was slightly higher than that of pure shape memory EP (90.34%). In addition, as can be seen from Figure 9 and (a) and 10(c), after 210 s, with the increase in temperature, the composite expanded by about 0.30 mm. After 280 s, it was heated above the glass state transition temperature, and the composite begins to recover its shape. The shape recovery rate gradually increased with the increase in GO content, and can finally return to the initial state. The shape recovery rates were close to 100%, which did not change with the change in GO content.

4.3 Mechanical property

In order to study the effect of GO doping on the mechanical properties of the SMGO/EP composites, the stress changes in shape memory process were obtained and explained.

Comparing the stress changes in the SMGO/EP composites with different volume fractions of GO in Figure 11, it can be seen that when the temperature was higher than T_g, the doping content of GO did not reveal significant effect on the stress with the increase in strain. When no

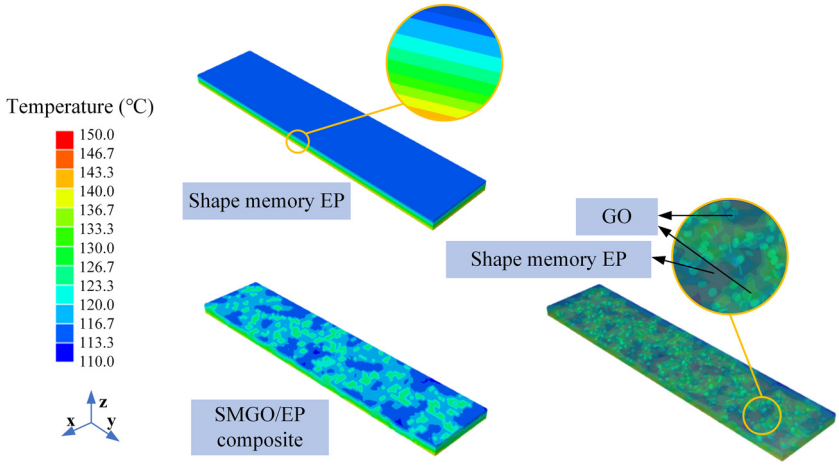

Figure 12: Comparison of temperature distribution of SMEP and SMGO/EP composites.

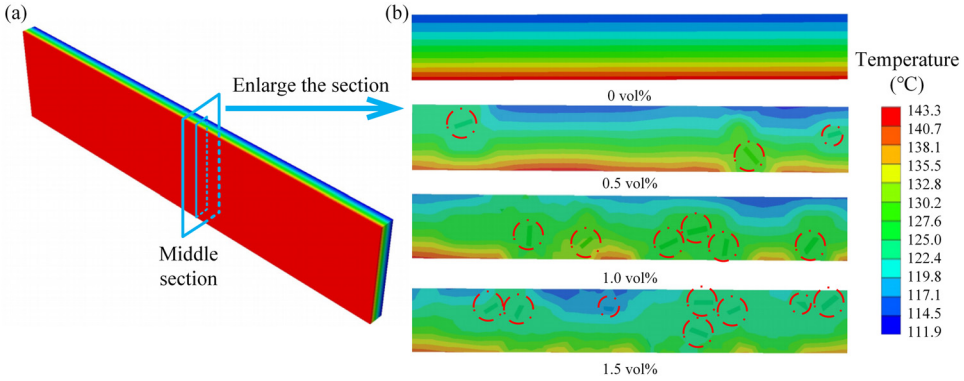

Figure 13: Middle section temperature distribution of SMGO/EP composites with 0 vol%, 0.5 vol%, 1.0 vol%, and 1.5 vol% GO contents.

GO was added, the stress increased from 0 to 1.90 MPa, while the stress increased from 0 to 2.51 MPa under the condition of 1.50 vol% GO doping content.

As the temperature gradually decreased below the glass transition temperature, the stress increased faster with the increase in the volume fraction of GO. When the temperature dropped to 30°C, the stress of pure shape memory EP was only 108.10 MPa. However, the stress of the sample with 0.50 vol% GO doping content was 133.18 MPa, which was increased by 23.20%. Compared with the samples with GO volume fraction of 1.00 vol% and 1.50 vol%, the stress of the samples was 144.60 MPa (increased by 33.77%) and 158.39 MPa (increased by 46.52%), respectively.

In the process of deformation, after removing the displacement load, the stress decreased instantaneously, but there was still a certain residual stress in the samples. As shown in Figure 11, the internal stress of SMEP was 3.63 Pa, while the internal stress generated by SMGO/EP composites was large. The internal stress of the sample with 0.50 vol% GO content was 24.60 MPa after removing the displacement load. The residual internal stress of the sample with GO volume fraction of 1.00 vol% was 35.48 MPa. When the volume fraction of GO was 1.50 vol%, the internal stress was 54.21 MPa. The above analysis showed that the internal stress of SMGO/EP composites increased with the increase in GO content after removing the displacement load. Then, in the recovery process, with the increase in temperature, the internal stress of SMGO/EP composites decreased linearly until the stress was completely eliminated. Furthermore, it can be obviously seen from Figure 10 that the attenuation rate of internal stress of SMGO/EP composite increased with the increase in the O content.

4.4 Heat transfer performance

In order to study the effect of GO doping on heat transfer process, the heat transfer process and results

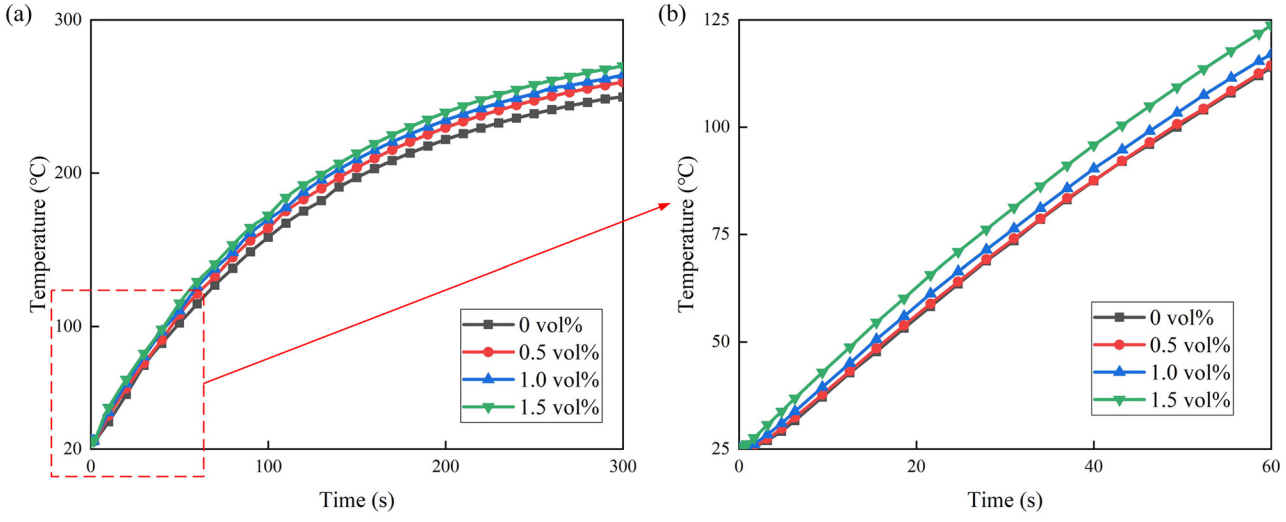

Figure 14: Temperature-rising curves with different GO contents: (a) 0–300 s, and (b) 0–60 s.

were analyzed. The contribution of GO to heat transfer enhancement was investigated.

Figure 12 shows the temperature distribution of SMGO/EP composites with 1.50 vol% GO content under the condition of heating for 60 s and heat source of 5,000 W/m^2. As can be seen from Figure 12, the temperature of SMEP gradually decreased along the z-axis direction. The bottom temperature can reach 142.61°C, and the surface temperature was 114.74°C. It can be seen from the figure that the surface temperature of GO doping areas was high, and the maximum temperature can reach 125.58°C with remarkable heat transfer effect. The temperature without GO doping was only 114.32°C. The average surface temperature of SMGO/EP composites was 123.77°C after heating for 60 s, which was 9.03°C higher than that of pure SMEP.

Figure 13 shows the section temperature distribution of SMGO/EP with different GO contents. The tagging positions in the cross section were randomly dispersed GO. It can be seen that the internal isotherms of the SMGO/EP composite were distributed in a curved shape, indicating that the temperature transfer was not uniform. The isotherm was obviously bent where the GO was distributed, accelerating the speed of heat transfer.

As can be seen from Figure 14(a), under the condition of initial temperature (25°C) and the external heat source (5,000 W/m^2), the surface temperature of the SMGO/EP composite increased linearly and then the temperature rise rate decreased gradually. After heating for 300 s, the heat transfer performance of the samples without GO doping was worst, and the average surface temperature was only 249.71°C. When the GO doping content was 0.50 vol%, 1.00 vol% and 1.50 vol%, the average surface temperature of the SMGO/EP composites corresponded to 259.42°C, 264.12°C and 269.97°C respectively.

Furthermore, it can be seen from Figure 14(b) that after heating for 60 s, when the doping content of GO was less than 0.50 vol%, the heat transfer speed did not increase significantly. With the further increase of GO doping, the heat transfer rate of SMGO/EP composite increased from 1.91 to 2.16°C/s, which the heat transfer capacity increased by 13.09%. This is due to the GO has an ideal structure suitable for heat transfer, and all carbon atoms are fixed on one layer by covalent bonds. When some atoms in GO contact with the heat source and begin to vibrate, the vibration will be quickly transferred to the surrounding atoms through the strong force of covalent bonds. The heat is transferred from one position of GO to another [65]. In addition, graphene relies on a special phonon mode for heat conduction. Graphene has a strong covalent bond between carbon and carbon, a small mass of carbon atoms, a high phonon velocity, and the thermal conductivity is directly proportional to the phonon velocity, so the thermal conductivity is high. The existence of a large number of high-density polymers in GO/EP nanocomposites is also the reason for the enhancement of thermal properties [66].

5 Conclusion

In this article, the shape memory properties, heat transfer characteristics, and mechanical properties of GO-doped SMEP were investigated by numerical simulation. Based on the micromorphology, the thermo-mechanical coupling model of SMGO/EP composites was established. The reliability of the simulation results was verified by experiments. Through data comparison, the shape fixing rate error was 2.33%, and the shape recovery rate was close to 100%. In the process of heat transfer, the temperature rise trend of simulation and experiment was consistent, and the maximum error was 6.04%. By analyzing the simulation data, the following experimental conclusions were obtained:

1) With the raising of the volume fraction of GO in the SMGO/EP composites, the maximum stress in the shape memory process increases accordingly. When the volume fraction of GO increases from 0 to 1.50 vol%, the maximum stress ranges from 108.10 MPa to 158.39 MPa; moreover, the stress of the SMGO/EP composites will not drop to 0 immediately after the displacement load was removed. The internal stress of the composites increases from 24.60 to 54.21 MPa with the GO doping from 0.50 to 1.50 vol% after the displacement load was removed. Moreover, the shape fixation rate of the SMGO/EP composites was directly proportional to the doping content of GO. When the volume fraction of GO was greater than 1.50 vol%, the shape fixation rate was greater than that of pure SMEP (90.34%). The doping of GO has small effect on the final shape recovery rate, which basically maintains 100% recovery. While, the shape recovery speed increased with the increase in the GO content.
2) The doping of GO in SMGO/EP composites significantly improves the heat transfer efficiency of the composites and forms a local high heat conduction region in the materials. Furthermore, the surface temperature of the composites with GO doping content of 1.50 vol% was 20.26°C higher than that of pure SMEP after heating for 300 s, increasing from 249.71°C to 269.97°C. The heat transfer rate of the SMGO/EP composites was 13.09% higher than that of pure SMEP after heating for 60 s, increasing from 1.91°C/s to

2.16°C/s. The addition of GO optimized the heat transfer performance of the SMGO/EP composites. Due to the excellent heat transfer performance of GO, the shape fixation rate and shape memory recovery rate of SMGO/EP composites were improved.

Funding information: This work was supported by Key Laboratory of Icing and Anti/De-icing of CARDC (Grant No. IADL20210407), Natural Science Foundation of Shandong Province (Grant No. ZR2019BEE068), and Natural Science Foundation of Guangdong Province (Grant No. 2020A1515111208). The authors thank the referees of this article for their valuable and very helpful comments.

Author contributions: Long Chen: conceptualization, data curation, writing-review & editing, and methodology. Qingbao Yang: formal analysis and methodology. Xue Yang: writing-original draft. Zhanqiang Liu: formal analysis and methodology. Qinghua Song: data curation and writing-review & editing. All authors have accepted responsibility for the entire content of this manuscript and approved its submission.

Conflict of interest: The authors state no conflict of interest.

References

[1] Maio ED, Mastrullo R, Mauro AW, Toto D. Thermal management of a multiple mini-channel heat sink by the integration of a thermal responsive shape memory material. Appl Therm Eng. 2014;62(1):113–22.
[2] Jiao P, Chen T, Xie Y. Self-adaptive mechanical metamaterials (SMM) using shape memory polymers for programmable postbuckling under thermal excitations. Compos Struct. 2021;256:113053.
[3] Li F, Liu L, Du L, Liu Y, Leng J. Mechanical analysis of a tip-loaded deployable truss based on shape memory polymer composite. Compos Struct. 2020;242:112196.
[4] Cui X, Chen J, Zhu Y, Jiang W. Natural sunlight-actuated shape memory materials with reversible shape change and self-healing abilities based on carbon nanotubes filled conductive polymer composites. Chem Eng J. 2020;382:122823.
[5] Wang B, Kang G, Yu C, Gu B, Yuan W. Molecular dynamics simulations on one-way shape memory effect of nanocrystalline NiTi shape memory alloy and its cyclic degeneration. Int J Mech Sci. 2021;211:106777.
[6] Zadafiya K, Kumari S, Chatterjee S, Abhishek K. Recent trends in non-traditional machining of shape memory alloys (SMAs): A review. CIRP J Manuf Sci Tec. 2021;32:217–27.
[7] Kumari S, Abhishek K. Study of machinability aspects of shape memory alloys: A critical review. Mater Today Proc. 2020;44:2214–7853.
[8] Adeodato A, Duarte BT, Monteiroa LS, Pachecoa PCL, Savib MA. Synergistic use of piezoelectric and shape memory alloy elements for vibration-based energy harvesting. Int J Mech Sci. 2020;194:106206.
[9] Xu B, Kang G. Phase field simulation on the super-elasticity, elastocaloric and shape memory effect of geometrically graded nano-polycrystalline NiTi shape memory alloys. Int J Mech Sci. 2021;201(2):106462.
[10] Moshkelgosha E, Mamivand M. Three-dimensional phase field modeling of fracture in shape memory ceramics. Int J Mech Sci. 2021;204:106550.
[11] Zaeem MA, Zhang N, Mamivand M. A review of computational modeling techniques in study and design of shape memory ceramics. Compu Mater Sci. 2019;160:120–36.
[12] Jetter J, Rohmer J, Wegner M, Quandt E. Fabrication of stable monoclinic zirconia-based ceramics. Ceram Int. 2021;47(6):8692–9696.
[13] Moshkelgosha E, Mamivand M. Concurrent modeling of martensitic transformation and crack growth in polycrystalline shape memory ceramics. Eng Fract Mech. 2021;241:107403.
[14] Yarali E, Taheri A, Baghani M. A comprehensive review on thermomechanical constitutive models for shape memory polymers. J Intel Mat Syst Str. 2020;31(10):1243–83.
[15] Meng H, Li G. A review of stimuli-responsive shape memory polymer composites. Polymer. 2013;54(9):2199–221.
[16] Bakhtiyari A, Baniasadi M, Baghani M. Development of a large strain formulation for multiple shape-memory-effect of polymers under bending. Int J Mech Sci. 2021;204:106550.
[17] Zeng H, Leng J, Gu J, Sun H. Modeling the thermomechanical behaviors of short fiber reinforced shape memory polymer composites. Int J Mech Sci. 2020;166(15):105212.
[18] Yan C, Yang Q, Li G. A phenomenological constitutive model for semicrystalline two-way shape memory polymers. Int J Mech Sci. 2020;177(1):105552.
[19] Zhao Q, Qi HJ, Xie T. Recent progress in shape memory polymer: New behavior, enabling materials, and mechanistic understanding. Prog Polym Sci. 2015;49:79–120.
[20] Dai L, Tian C, Xiao R. Modeling the thermo-mechanical behavior and constrained recovery performance of cold-programmed amorphous shape-memory polymers. Int J Plast. 2020;127:102654.
[21] Chen S, Hu J, Zhuo H. Properties and mechanism of two-way shape memory polyurethane composites. Compos Sci Technol. 2010;70(10):1437–43.
[22] Liu Y, Han C, Tan H, Du X. Thermal, mechanical and shape memory properties of shape memory epoxy resin. Mater Sci Eng A. 2010;527(10–11):2510–4.
[23] Li J, Zhang Z, Zhang Y, Sun F, Wang D, Wang H, et al. Synergistic effect of lignin and ethylene glycol crosslinked epoxy resin on enhancing thermal, mechanical and shape memory performance. Int J Biol Macromol. 2021;192:516–24.
[24] Capricho JC, Fox B, Hameed N. Multifunctionality in Epoxy Resins. Polym Rev. 2020;60:1–41.
[25] Zhou X, Ma B, Wei K, Wang X. Preparation of shape memory epoxy resin for asphalt mixtures and its influences on the main pavement performance. Constr Build Mater. 2021;267:121055.

[26] Liu Y, Han C, Tan H, Du X. Thermal, mechanical and shape memory properties of shape memory epoxy resin. Mater Sci Eng A. 2010;527(10–11):2510–4.
[27] Wu X, Yang X, Zhang Y, Huang W. A new shape memory epoxy resin with excellent comprehensive properties. J Mater Sci. 2016;51(6):3231–40.
[28] Sun H, Liu Y, Tan H, Du X. A new method to improve the stability, tensile strength, and heat resistant properties of shape-memory epoxy resins: Two-stages curing. J Appl Polym Sci. 2014;131(4):1–7.
[29] Verma DK, Purohit R, Rana RS, Purohiit S, Patel KK. Enhancement of the properties of shape memory polymers using different nano size reinforcements – A review. Mater Today Proc. 2020;26(2):3037–42.
[30] Asar A, Irfan MS, Khan KA, Zaki W, Umer R. Self-sensing shape memory polymer composites reinforced with functional textiles. Compos Sci Technol. 2021;109219.
[31] Ji Q, Chen M, Wang X, Wang L, Feng L. Optimal shape morphing control of 4D printed shape memory polymer based on reinforcement learning. Robot CIM-Int Manu. 2022;73:102209.
[32] Li H, Zhong J, Meng J, Xian G. The reinforcement efficiency of carbon nanotubes/shape memory polymer nanocomposites. Compos B Eng. 2013;44(1):508–16.
[33] Yu K, Liu Y, Leng J. Conductive shape memory polymer composite incorporated with hybrid fillers: electrical, mechanical, and shape memory properties. J Intell Mater Syst Struct. 2011;22(4):369–79.
[34] Liu Y, Gall K, Dunn ML, Mccluskey P. Thermomechanics of shape memory polymer nanocomposites. Mech Mater. 2004;36(10):929–40.
[36] Kalita H, Karak N. Bio-based hyperbranched polyurethane/Fe_3O_4 nanocomposites as shape memory materials. Polym Adv Technol. 2013;24(9):819–23.
[35] Ohki T, Ni Q, Ohsako N, Iwamoto M. Mechanical and shape memory behavior of composites with shape memory polymer. Compos Part A Appl Sci Manuf. 2004;35(9):1065–73.
[37] Wei K, Zhu G, Tang Y, Li X, Liu T, Niu L. An investigation on shape memory behaviours of hydro-epoxy/glass fibre composites. Compos B Eng. 2013;51:169–74.
[38] Li F, Leng J, Liu Y, Remillat C, Scarpa F. Temperature dependence of elastic constants in unidirectional carbon fiber reinforced shape memory polymer composites. Mech Mater. 2020;148:103518.
[39] Rana S, Karak N, Cho JW, Kim YH. Enhanced dispersion of carbon nanotubes in hyperbranched polyurethane and properties of nanocomposites. Nanotechnology. 2008;19(49):495707.
[40] Abishera R, Velmurugan R, Gopal KVN. Reversible plasticity shape memory effect in epoxy/CNT nanocomposites – A theoretical study. Compos Sci Technol. 2017;141:145–53.
[41] Jung YC, Kim JH, Hayashi T, Kim YA, Endo M, Terrones M, et al. Fabrication of Transparent, Tough, and Conductive Shape-Memory Polyurethane Films by Incorporating a Small Amount of High-Quality Graphene. Macromol Rapid Commun. 2012;33(8):628–34.
[42] Martin-Gallego M, Bernal MM, Hernandez M, Verdejo R, Lopez-Manchado MA. Comparison of filler percolation and mechanical properties in graphene and carbon nanotubes filled epoxy nanocomposites. Eur Polym J. 2013;49(6):1347–53.
[43] Liu P, Lam A, Fan Z, Tran TQ, Duong HM. Advanced multifunctional properties of aligned carbon nanotube-epoxy thin film composites. Mater Des. 2015;87:600–5.
[44] Datta S, Henry TC, Sliozberg YR, Lawrence BD, Chattopadhyay A, Hall AJ. Carbon nanotube enhanced shape memory epoxy for improved mechanical properties and electroactive shape recovery. Polymer. 2021;212:123158.
[45] Wang E, Dong Y, Ialam MZ, Yu L, Liu F, Chen S, et al. Effect of graphene oxide-carbon nanotube hybrid filler on the mechanical property and thermal response speed of shape memory epoxy composites. Compos Sci Technol. 2019;169:209–16.
[46] Liu Y, Guo Y, Zhao J, Chen X, Zhang H, Hu G, et al. Carbon fiber reinforced shape memory epoxy composites with superior mechanical performances. Compos Sci Technol. 2019;177:49–56.
[47] Lu H, W. Huang. Synergistic effect of self-assembled carboxylic acid-functionalized carbon nanotubes and carbon fiber for improved electro-activated polymeric shape-memory nanocomposite. Applied Physics Letters. 2013;102(23):231910.
[48] Lu H, F. Liang and J. Gou. Nanopaper Enabled Shape-Memory Nanocomposite with Vertically Aligned Nickel Nanostrand: Controlled Synthesis and Electrical Actuation. Soft Matter. 2011;7(16):7416–23.
[49] Sun R, Li L, Feng C, Kitipornchai S, Yang J. Tensile property enhancement of defective graphene/epoxy nanocomposite by hydrogen functionalization. Compos Struct. 2019;224:111079.
[50] Hussein A, Kim B. Micromechanics based FEM study on the mechanical properties and damage of epoxy reinforced with graphene based nanoplatelets. Compos Struct. 2019;215:266–77.
[51] Yu Z, Wang Z, Li H, Teng J, Xu L. Shape memory epoxy polymer (SMEP) composite mechanical properties enhanced by introducing graphene oxide (GO) into the matrix. Materials. 2019;12(7):1107.
[52] Chen L, Li W, Liu Y, Leng J. Nanocomposites of epoxy-based shape memory polymer and thermally reduced graphite oxide: Mechanical, thermal and shape memory characterizations. Compos B Eng. 2016;91:75–82.
[53] Wang Y, Tian W, Xie J, Yan L. Thermoelectric responsive shape memory graphene/hydro-epoxy composites for actuators. Micromachines. 2016;7(8):145.
[54] Wang E, Wu Y, Islam MZ, Dong Y, Zhu Y, Liu F, et al. A novel reduced graphene oxide/epoxy sandwich structure composite film with thermo-, electro- and light-responsive shape memory effect. Mater Lett. 2019;238:54–7.
[55] Liu T, Liu L, Yu M, Li Q, Zeng C, Lan X, et al. Integrative hinge based on shape memory polymer composites: materials, design, properties and application. Compos Struct. 2018;206:164–76.
[56] Fan P, Chen W, Zhao B, Hu J, Gao J, Fang G, et al. Formulation and numerical implementation of tensile shape memory process of shape memory polymers. Polymer. 2018;148:370–81.
[57] Diani J, Gilormini P, Frédy C, Rousseau I. Predicting thermal shape memory of crosslinked polymer networks from linear viscoelasticity. Int J Solids Struct. 2012;49(5):793–9.
[58] Shokrgozar M, Tizfahm A, Mozaffari A. Finite element analysis of viscoelastic laminates embedded with shape-memory-alloy

wires under low-velocity impact considering large deflection. Mech Mater. 2021;156:103810.
[59] He G, Liu Y, Deng X, Fan L. Constitutive modeling of viscoelastic-viscoplastic behavior of short fiber reinforced polymers coupled with anisotropic damage and moisture effects. Acta Mech Sin. 2019;35(3):496–506.
[60] Landel RF. A Two-Part Tale: The WLF Equation and Beyond Linear Viscoelasticity. Rubber Chem Technol. (2006);79(3):381–401.
[61] Mishnaevsky L, Dai G. Hybrid and hierarchical nanoreinforced polymer composites: Computational modelling of structure-properties relationships. Compos Struct. 2014;117(1):156–68.
[62] Chai Y, Liang S, Zhou Y, Lin L, Fu F. 3D microscale heat transfer model of the thermal properties of wood-metal functional composites based on the microstructure. Materials. 2019;12(17):2709.
[63] McClung AJW, Tandon GP, Baur JW. Effects of loading rate on the relaxation and recovery ability of an epoxy-based shape memory polymer. Fluid. 2017;2:13–5.
[64] Monzón MD, Paz R, Pei E, Ortega F, Suárez LA, Ortega Z, et al. 4D printing: processability and measurement of recovery force in shape memory polymers. Int J Adv Manuf Technol. 2017;89(5–8):1827–36.
[65] Li A, Zhang C, Zhang Y. Thermal conductivity of graphene-polymer composites: mechanisms, properties, and applications. Polymers. 2017;9(9):437.
[66] Shiu SC, Tsai JL. Characterizing thermal and mechanical properties of graphene/epoxy nanocomposites. Compos B Eng. 2014;56:691–7.